

Simulations of Classical Three-Body Thermalization in One Dimension

M. Eltohfa,* Xinghan Wang, Colton M. Griffin, and F. Robicieux†

Department of Physics and Astronomy, Purdue University, West Lafayette, Indiana 47906 USA

(Dated: March 4, 2024)

One-dimensional systems, such as nanowires or electrons moving along strong magnetic field lines, have peculiar thermalization physics. The binary collision of point-like particles, typically the dominant process for reaching thermal equilibrium in higher dimensional systems, cannot thermalize a 1D system. We study how dilute classical 1D gases thermalize through three-body collisions. We consider a system of identical classical point particles with pairwise repulsive inverse power-law potential $V_{ij} \propto 1/|x_i - x_j|^n$ or the pairwise Lennard-Jones potential. Using Monte Carlo methods, we compute a collision kernel and use it in the Boltzmann equation to evolve a perturbed thermal state with temperature T toward equilibrium. We explain the shape of the kernel and its dependence on the system parameters. Additionally, we implement molecular dynamics simulations of a many-body gas and show agreement with the Boltzmann evolution in the low density limit. For the inverse power-law potential, the rate of thermalization is proportional to $\rho^2 T^{\frac{1}{2} - \frac{1}{n}}$ where ρ is the number density. The corresponding proportionality constant decreases with increasing n .

I. INTRODUCTION

A. Technological Motivation

With the advance of technology, very thin systems can be produced that can be approximated as one-dimensional (1D). Examples of 1D gases include quantum-wires made of GaAs [1] or carbon nanotubes [2]. Other examples come from plasma physics where electrons are confined to move along strong magnetic field lines [3], or isolated, far-from-equilibrium, Bose gases [4]. Thus, the properties of 1D systems are of some interest.

One dimensional confinement considerably affects system properties, such as thermalization process [5], enhanced correlations and collective behavior [6], and anomalous transport and diffusion [7]. In the present work, we study the rate of thermalization of certain 1D systems. This rate measures how fast the equilibrium state is reached if the system starts from a non-equilibrium state. From another perspective, it measures how fast the system loses memory of its initial state.

Unique features of 1D thermalization have been demonstrated. Optical measurements have shown that carrier relaxation is much slower in quantum wires than in bulk and two-dimensional forms [8]. Additionally, molecular dynamical (MD) simulations of a 1D line of electrons have shown the system thermalizes in the order of $10 ns$ [5], which is a relatively slow rate. On the other hand, the dynamics of thermalization of quasi-1D systems, consisting of nearly decoupled chains, was shown to exhibit non-exponential approach to equilibrium [9].

For this paper, we simulate the interaction of classical point-like particles that are confined to move in 1D. We define the thermalization rate by how fast a special velocity of a particle irreversibly diffuses into the distribution of the rest of the system. With this definition,

we show that the 1D gases under study exhibit very slow thermalization rates.

B. Theoretical Motivation

1. Two-body thermalization

In the kinetic theory of 3D gases, thermalization through binary collisions has been thoroughly studied [10]. Binary collisions are the dominant interaction if the gas is dilute; many-particle collisions are suppressed by powers of the density [11]. Although a binary collision is tightly constrained by several conservation conditions, there is freedom for the particles to change their directions based on their impact parameter.

In the center of mass frame of the two colliding bodies, the equations of motion can be integrated and a non-zero differential cross-section can be obtained. Subsequently, the cross section determines the rate of scattering from and into a tiny volume in coordinate-velocity space of the one-particle distribution. These rates can be used in the Boltzmann Equation to propagate the distribution [10]. By Boltzmann's H theorem, a non-zero cross section guarantees the thermalization of the system to equilibrium. Binary collisions also lead to thermalization in 2D although the details are different.

Thermalization through binary collisions, however, does not work in a 1D gas of identical point like particles. Consider two particles of mass m elastically colliding with incoming velocities v_1, v_2 , and outgoing velocities w_1 and w_2 . Conservation of energy and momentum must hold. This, in 1D, entails two equations which completely determine that $w_2 = v_1$ and $w_1 = v_2$. This is a trivial swapping that leads to the same velocities and, therefore, to an unchanged velocity distribution[5].

The triviality of the binary collision in 1D hinges on two assumptions [5]: 1- the dispersion relation is parabolic which is well established. 2- there is no exchange of momentum with the substrate (the crystal or

* meltohfa@purdue.edu

† robichf@purdue.edu

the medium the particles live in). The latter assumption works well in regimes of energy less than $1eV$ for crystal spacing $10^{-10}m$, or if the particles live in 1D vacuum. In this work, we assume that the particles are constrained to move on a ring or a line with no external forces.

2. Many-body thermalization in 1D

It was shown in [5] that many-body Coulomb scattering can thermalize a one-dimensional electron gas in a single-subband GaAs quantum wires. This was done through classical molecular dynamics (MD) simulations. In the study, the gas is dense enough such that the mean potential energy is of the order of the mean kinetic energy $\sim 100K \sim 10meV$. It was calculated that the relaxation time is of order $10ns$ and increases rapidly for lower densities.

3. Three-body thermalization in 1D

Since binary collisions cannot thermalize a 1D system, we study thermalization through the next simplest process, the three-body (ternary) collisions. In very dilute gases, which is our main focus, the ternary collision is dominant over the higher order collisions. The ternary collision is generally non-trivial and can generate new velocity states. For long-range interacting homogeneous 1D systems, it was shown that they can thermalize through 3-body effects, but their relaxation is drastically slowed down [12]. The 3-body problem, however, is non-integrable [13] (except in very special cases [14]), so we study its trajectories numerically.

Three-body thermalization has also been addressed in [15] for a model problem. The scattering rate from a triple of initial momenta to a triple final momenta was assumed for simplicity to be constant as long as the incoming momenta and the outgoing momenta satisfy energy and momentum conservation. In such cases, the Boltzmann Eq. (B1) is exactly solvable. This constant scattering rate, however, was not derived from an inter-particle potential energy. Additionally, it was found that the rate of collisions, and hence the rate of thermalization, goes as ρ^2 but is not affected by temperature or the average kinetic energy. With the rates computed from an inter-particle potential, we will show that if we start from a quasi-thermal distribution of temperature T , the rate of thermalization depends not only on ρ but also on T .

C. Goal and Plan

In the present paper, we first introduce a model of a 1D gas on a ring and a model of thermalization. We consider a system with pairwise inverse power potential with power $n \geq 2$. This potential is formally long-range,

since any particle can affect any other particle with non-zero force. But for low densities and high temperatures, which we assume, this force is small enough that long-range effects can largely be ignored [16]. We consider the evolution of a ‘delta-perturbed’ thermal state. Previous studies [5], [9] considered the evolution of a bimodal distribution or a modified Gaussian [16].

Second, we implement MD simulations and discuss the scaling of the thermalization rate, which we define as the initial rate of the spread of the perturbation. Third, using Monte Carlo simulations, we calculate a three-body collision kernel for the inverse power potential and the Lennard-Jones potential. Using the kernel information, we show how the transition rates scale with ρ and T and compute the thermalization rate for a range of parameters. Fourth, the collision kernel is used in the Boltzmann equation to evolve the perturbation and this method is shown to be in agreement with the MD simulations. Finally, we discuss the shape of the kernel and how it changes with the inverse potential power n .

II. GAS AND THERMALIZATION MODEL

We consider N identical particles of mass m constrained to move on a ring of radius R as in Fig. 1 with pairwise repulsive inverse power-law potential

$$U(d) = \epsilon \left(\frac{l_0}{d} \right)^n, \quad (1)$$

where d is the pairwise separation, l_0 is the basic unit of length at which the potential energy is equal to some interaction strength $\epsilon > 0$, and n is an even integer ≥ 2 .

The locations of the particles are parameterized by the angles ϕ_i and the mutual distance between particles i and j is

$$d_{ij} = 2R \sin \left(\frac{|\phi_i - \phi_j|}{2} \right). \quad (2)$$

The energy of the system is

$$E = \sum_{i=1}^N \frac{mR^2 \omega_i^2}{2} + \epsilon \left(\frac{l_0}{2R} \right)^n \sum_{i,j>i}^N \left[\sin \left(\frac{\phi_i - \phi_j}{2} \right) \right]^{-n}, \quad (3)$$

where ω_i is the angular velocity of particle i .

We consider a thermal initial condition sampled from a Boltzmann distribution with temperature T . In particular, the initial velocity $v(t=0) = R\omega(t=0)$ of a particle follows the Maxwell-Boltzmann statistics with probability density function:

$$f_0(v) = \frac{1}{\sqrt{2\pi v_{th}^2}} e^{-v^2/2v_{th}^2} \quad (4)$$

where $v_{th} = \sqrt{kT/m}$ is the velocity scale set by the temperature. k is the Boltzmann constant.

In this work, we assume high enough T and small enough number density, $N/(2\pi R)$, so that the average kinetic energy is much greater than the potential energy (unlike in Ref. [5], where the energies are comparable). In this regime, correlations between positions of the particles, higher order collisions, and collective effects can be ignored as in Ref. [16].

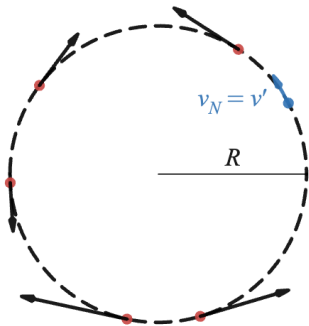


FIG. 1. Particles on a ring of radius R . All but one particle are initialized from a thermal distribution. The ‘special’ particle (in blue) is initialized with a special velocity v' . The special particle represents a perturbation to the thermal state.

We choose a ring to represent the 1D system instead of a line so that particles do not escape to infinity under repulsive forces. Modeling a line would require a confining potential which leads to the particles at the edges experiencing a different environment from those in the center of the range. We are aware of the two artifacts of the ring: curvature and periodic effects. To simulate a particular linear number density, ρ , we tackle the ring effects by doubling R and the number of thermal particles, $N - 1$, until our results converge.

We consider a perturbation to the thermal state by starting the N^{th} particle at velocity v' as in Fig. 1. We refer to such a particle as the ‘special’ particle and its velocity as the ‘special velocity’, while we refer to the rest of the particles as ‘thermal’. The velocity probability density function of the total system is

$$f(v, t = 0) = \frac{N-1}{N} f_0(v) + \frac{1}{N} h(v, t = 0), \quad (5)$$

where $h(v, t)$ is the normalized perturbation (integral over v is 1) such that

$$h(v, t = 0) = \delta(v - v'). \quad (6)$$

If we introduce the scaled velocity $u = v/v_{th}$, then the

normalized (integral over u is 1) initial distribution is

$$f(u, t = 0) = \frac{N-1}{N} \frac{1}{\sqrt{2\pi}} e^{-\frac{u^2}{2}} + \frac{1}{N} \delta(u - u'), \quad (7)$$

Our goal is to study the evolution of h . According to the Boltzmann H -theorem [10], the steady state distribution $f(v, \infty)$, and therefore $h(v, \infty)$, is the equilibrium distribution f_0 . This is strictly true in the thermodynamic limit $N \rightarrow \infty$. For finite N , however, the steady state has a slightly different temperature $T_f \simeq (N-1 + u'^2)T/N \approx T$ for large N , which is a result of energy conservation. We run many MD simulations where the $N - 1$ thermal particles are randomly chosen from a thermal distribution. Averaging over these many runs gives an average $h(u, t)$.

From our MD simulations (as described in Appendix A), the average $h(u, t)$ starting from $\delta(u)$ is shown for two times in Fig. 2. As expected, the perturbation’s peak height decreases and its width increases as the system evolves. The times shown are early in the thermalization process where the population only spreads to small velocities ($|u| < 0.06$). However, the cusp feature of the delta function is maintained throughout this time period, which is an indication that the gas is far from equilibrium. The parameters of the simulated gas are $l_0 = 1 \mu\text{m}$, $\epsilon = 1 \text{ eV}$, $kT = 100 \text{ meV}$, $m = m_e$ (mass of the electron), $n = 6$, $N = 41$, and $R = 6400 \mu\text{m}$. The times shown are $t_f = 960, 3200 \text{ ns} = 0.48, 1.6 \times 10^{-4}/\Gamma$ (Γ being the rate of thermalization defined in Eq. (8)).

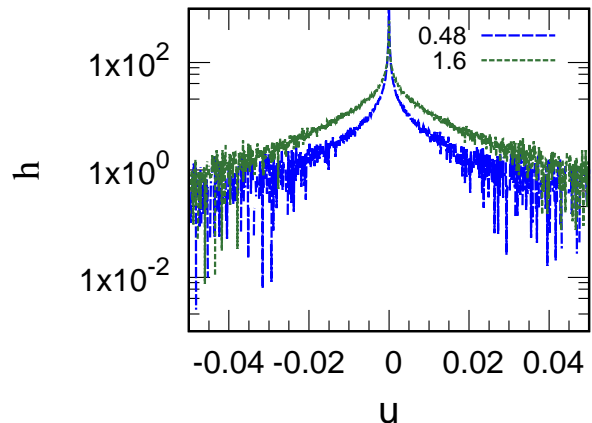


FIG. 2. MD simulated evolution of the perturbation initially $\delta(u)$ for parameters $N = 41$ and $R = 6400 \mu\text{m}$. The times shown are $t_f = 960, 3200 \text{ ns} = 0.48, 1.6 \times 10^{-4}/\Gamma$, and the x -axis is the scaled velocity u . Comparing the distribution at these two time instants and at $t = 0$ (not shown), the perturbation width increases with time as its height drops.

To investigate the rate of thermalization, we introduce Γ to be the initial rate of change of the variance of the perturbation:

$$\Gamma = \left. \frac{d\langle (u - u')^2 \rangle_h}{dt} \right|_{t=0}. \quad (8)$$

This definition of Γ implies that if the perturbation continues spreading at the initial rate, then it takes time of order $1/\Gamma$ for the perturbation $h(u)$ to reach variance ~ 1 , i.e., the special particle reaching the temperature of the bath. In the rest of the paper, we show how Γ depends on the system parameters $\{R, N, m, T, l_0, \epsilon, n, u'\}$. To extract this dependence, we do MD simulations for different parameter sets; however, as argued in Appendix A, such N -body simulations are computationally very expensive when N is large or the propagation time, t_f , is large.

III. BOLTZMANN EVOLUTION OF THE GAS

A more efficient method to study Γ is to consider the simpler process by which our system thermalizes, the ternary collision. By knowing the frequency of such collisions and how they change the particle velocities, we can propagate the velocity distribution in time. The recipe of such method is the Boltzmann equation. For those reasons, we choose to focus on the Boltzmann method and limit ourselves to a few MD simulations. In particular, we use the MD simulations to extract some preliminary scaling for Γ and as a benchmark to verify our Boltzmann calculations.

The Boltzmann evolution is an example of a continuous time Markov chain in which the next step distribution is only dependent on the current distribution. If the perturbation is initially localized at v' , $h(v, 0) = \delta(v - v')$, then after infinitesimal duration dt , the perturbation becomes

$$h(v, dt) = \delta(v - v') + dt K_{v' \rightarrow v}, \quad (9)$$

where the kernel $K_{v' \rightarrow v}$ is the rate of transitioning from velocity v' to the range between $v - \frac{\Delta v}{2}$ and $v + \frac{\Delta v}{2}$ per Δv in the limit $\Delta v \rightarrow 0$. After a finite time, the perturbation delocalizes to a continuous range of v ; the evolution equation then becomes

$$h(v, t + dt) = h(v, t) + dt \int_{-\infty}^{\infty} K_{v' \rightarrow v} h(v', t) dv' \quad (10)$$

Numerically, we work with a discretized version of the distribution and the kernel. The velocity axis is divided into bins of width Δv , which we choose as a fraction of v_{th} . Each bin is labeled by its center velocity $v_i = i\Delta v$ and extends from $v_i - \frac{\Delta v}{2}$ to $v_i + \frac{\Delta v}{2}$. Equation (10) becomes

$$h_i(t + dt) \approx h_i(t) + dt \sum_{j=-\infty}^{j=\infty} K_{v_j \rightarrow v_i} h_j(t), \quad (11)$$

where $h_i \Delta v$ is the population in bin v_i ,

To ensure that the population (particle number) is conserved, the scattering rate out of velocity bin v_i ($K_{v_i \rightarrow v_i}$) must equal the scattering rate into any other velocity v_j .

That is,

$$K_{v_i \rightarrow v_i} = - \sum_{j \neq i} K_{v_i \rightarrow v_j}. \quad (12)$$

where the minus sign indicates that population is lost from bin v_i .

A. Monte Carlo Simulation of K

To calculate the transition rates $K_{v' \rightarrow v}$, we focus on the special particle with velocity v' and treat the rest of the system as a thermal bath of temperature T and number density ρ . Through a Monte Carlo (MC) simulation on a line [17], we simulate the possible collisions the special particle (referred to as particle 1) encounters with two other thermal particles (referred to as particles 2 and 3).

The set of all possible 3-body collisions can be determined by first changing to an inertial frame moving with velocity v' where the special particle is at rest before the collision. In this frame, particle 1 is initialized with velocity $v_1 = 0$ at the origin $x = 0$. We consider an observation region of length L centered around the special particle. In a small time duration, there is a probability that a thermal particle (particle 2 or 3) will enter the observation region from either side at $x = \pm L/2$ with some velocity (v_2 or v_3). We model the ‘launching’ of the particles into the observation region as a Poisson process with rate r . The rate r determines the distribution for the delay Δt between the launched particles. By studying the phase space distribution of a particle in the considered thermal bath, we determine r and the statistics of the launched particles. These statistics and the steps of the algorithm are described in Appendix C.

IV. RESULTS

A. Scaling Behavior of the N -body Gas

In this section, we extract the 3-body scaling using MD simulations. Before presenting the results of the simulations, we predict the scaling by analyzing the equations of motion of the N -body gas on the ring. The equations of motion follow from the energy in Eq. (3):

$$mR \frac{d\omega_i}{dt} = \sum_{j \neq i} \frac{n\epsilon}{2} \frac{\left(\frac{l_0}{2R}\right)^n}{R \left[\sin\left(\frac{\phi_i - \phi_j}{2}\right)\right]^{n+1}} \cos\left(\frac{\phi_i - \phi_j}{2}\right),$$

$$\frac{d\phi_i}{dt} = \omega_i. \quad (13)$$

These equations can be scaled resulting in equations of motion independent of all dimensional parameters.

We reduce the number of parameters by first identifying the length, time, and angular velocity scales. The

angular velocity scale comes naturally from the thermal velocity: $\omega_{th} = v_{th}/R$, where v_{th} was defined in the context of Eq. (4). The dynamical time scale is proportional to the average orbital time: $t_d = 1/\omega_{th}$. The simple form of the inverse power potential is utilized to find the length scale. The pairwise interaction can be rewritten as

$$U(d) = kT \left(\frac{l}{d} \right)^n, \quad (14)$$

where

$$l = l_0 \left(\frac{\epsilon}{kT} \right)^{\frac{1}{n}} \quad (15)$$

is the length scale (closest approach distance) set by the temperature.

If the scaled angular velocity is $\tilde{\omega} = \omega/\omega_{th}$ and the scaled time is $\tilde{t} = t/t_d$ then

$$\begin{aligned} \frac{d\tilde{\omega}_i}{d\tilde{t}} &= \sum_{j \neq i}^N \frac{n}{2} \frac{c}{\left[\sin \left(\frac{\phi_i - \phi_j}{2} \right) \right]^{n+1}} \cos \left(\frac{\phi_i - \phi_j}{2} \right), \\ \frac{d\phi_i}{d\tilde{t}} &= \tilde{\omega}_i, \end{aligned} \quad (16)$$

where

$$c = \left(\frac{l}{2R} \right)^n. \quad (17)$$

The dynamics of two systems in terms of the scaled variables is identical if their corresponding c , n , and N parameters are the same. The disappearance of the energy scales (kT or ϵ) in the scaled Eq. (16) is owed to the scale invariance of the inverse power potential. In Sec. IV F, we demonstrate how the energies re-enter the dynamics if we consider other potentials such as the Lennard-Jones potential, which does not lead to scaled equations of motion.

From the definition of l in Eq. (15), kT scales as l^{-n} . Furthermore, the density ρ of the particles for a given N scales as R^{-1} . Thus, c scales as $T^{-1}\rho^n$. If one scales $\rho \rightarrow a\rho$ and $T \rightarrow a^n T$, c remains the same. Therefore, the scaled dynamics (Eq. (16) alongside the scaled initial conditions) remains the same. Given this constraint, one can show that the most general time scale must be proportional to $\rho^{-s} T^{-(\frac{1}{2} - \frac{s-1}{n})}$, where s is an integer. These time scales are also obtainable from dimensional analysis of the system's parameters. The most general rate γ is thus governed by terms of the form (rewritten using l and v_{th})

$$\gamma \sim \rho^s l^{s-1} v_{th}. \quad (18)$$

Cases where $s \geq 0$ have physical interpretations. $s = 0$ gives a time scale $t_c = l/v_{th}$ which is proportional to the interaction time *during* a binary collision. $s = 1$ gives the dynamical time scale t_d which is proportional to the mean time *between* binary collisions. Similarly, $s = 2$ gives

the rate of ternary interactions. The probability that two particles existing in an interaction region of length l scales as ρl , and the rate of a third particle entering this region to interact with the other two particles is ρv_{th} . Thus the ternary interaction rate scales as $\rho^2 l v_{th}$.

For each additional particle colliding, there is one more factor of ρl . For small densities where $\rho l \ll 1$, the relevant term for thermalization is the 3-body interaction term since the two body collision is trivial. In the thermodynamic limit $N \rightarrow \infty$, we get the scaling of the 3-body thermalization rate in Eq. (8):

$$\Gamma = a_n \rho^2 l v_{th}, \quad (19)$$

where a_n is a dimensionless quantity depending only on n in Eq. (1).

From Eq. (19), we expect that the evolution rate is proportional to $\rho^2 T^{1/3}$ for $n = 6$. To test this scaling, we compare a gas with density ρ and temperature T evolving for time t_f with two other cases: $2\rho, T$ evolving for $t_f/4$ and $2\rho, 8T$ evolving for $t_f/8$. Figure 3 shows the evolved distribution in the three cases. All three curves are the same within statistical uncertainty, which confirms the predicted scaling.

Parameters used in the MD simulation are $N = 161$ particles for three cases: $R = 51200 \mu m$, $kT = 100 meV$, $t_f = 12800 ns$; $R = 25600 \mu m$, $kT = 100 meV$, $t_f = 3200 ns$; and $R = 25600 \mu m$, $kT = 800 meV$, $t_f = 1600 ns$. In all cases, $l_0 = 1 \mu m$, $\epsilon = 1 eV$, $m = m_e$, and $n = 6$. In all cases, the final time $t_f = 1.6 \times 10^{-4} / \Gamma$ as computed from Eq. (19).

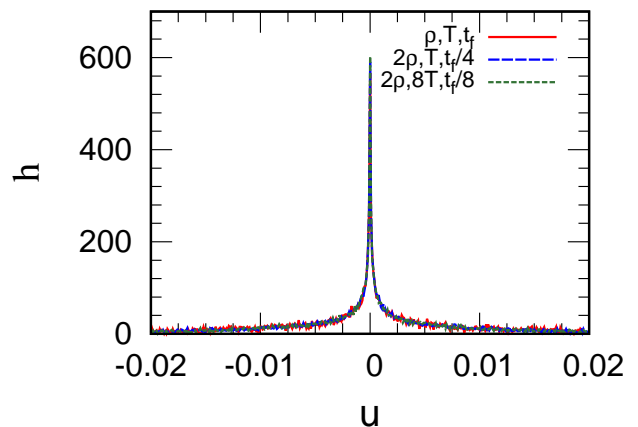


FIG. 3. Three different parameter sets with respective $t_f \propto 1/(\rho^2 T^{1/3})$ give identical final distributions.

B. Scaling of the Collision Kernel K

A necessary condition for Eq. (10) to reproduce the MD evolution is that $K\Delta v$ as computed from the MC simulations must have the scaling of Γ in Eq. (19). We show that K indeed has the desired scaling under the

assumption that $\rho l \ll 1$, where l is defined in Eq. (15). If we define $\tilde{x} = x/l$, $u = v/v_{th}$, and $\tilde{t} = tv_{th}/l$, then those equations are

$$\frac{du_i}{d\tilde{t}} = \sum_{j=0, j \neq i}^2 \frac{n}{(\tilde{x}_i - \tilde{x}_j)^{n+1}}, \quad (20)$$

$$\frac{d\tilde{x}_i}{d\tilde{t}} = u_i. \quad (21)$$

Since the length scale is l , we set the length of the region L to scale with l . In our calculations, for example, we get converging results for the scaling of K at $L = 90l$ and $\rho l = 5 \times 10^{-5}$. The scaled dynamics (Eq. (20)) of a single trajectory only depends on n ; that is, scaled initial velocities and positions map to scaled final velocities and positions irrespective of ρ and T . If ρ or T changes, the rate r of launching changes according to Eq. (C1), and the average time spent in the observation region scales as l/v_{th} .

Not all simulated trajectories result in a non-trivial change in velocities. Only trajectories where the two launched particles coincide for some time in the region result in effective 3-body scattering. Otherwise, the collision is just a sequence of binary collisions that only swap velocities just like in a Newton's cradle.

This coincidence rate Γ_{coin} is calculated according to a Poisson process with rate r and observation time window $t_{ob} \propto l/v_{th}$.

$$\begin{aligned} \Gamma_{coin} &= \frac{\text{probability of two arrivals}}{t_{ob}} \\ &= \frac{(rt_{ob})^2 e^{-rt_{ob}}}{2t_{ob}} \approx \frac{1}{2} r^2 t_{ob} \propto \rho^2 v_{th} l \end{aligned} \quad (22)$$

The coincidence rate (rate of effective 3-body collisions) is proportional to the rate of thermalization, Γ , in Eq. (19) and the kernel $K\Delta v$, which we verify by introducing the dimensionless scaled kernel

$$G_{u' \rightarrow u} \Delta u = \frac{K_{v' \rightarrow v} \Delta v}{\rho^2 l v_{th}}, \quad (23)$$

where $u = v/v_{th}$. We show in Fig. 4 that G is independent of T and ρ given that $\rho l \ll 1$, $L/l \gg 1$. The scaled kernel $G_{0 \rightarrow u}$ (denoted by G in the y-axis label) is plotted against the scaled velocity $u = v/v_{th}$. The parameters used in the MC simulations are $v' = 0$ (initially stationary special particle), $n = 6$, $kT = 100 \text{ meV}$, $l_0 = 1 \mu\text{m}$, $\epsilon = 1 \text{ eV}$, $m = m_e$, bin width $\Delta v = 0.1 v_{th}/2000$, $\rho l = 5 \times 10^{-5}$ and $L = 90l$, where l is defined in Eq. (15).

Since G is independent of ρ and T , the kernel scales like $K\Delta v \propto \rho^2 l v_{th}$. Although we do not explicitly show the scaling with the other parameters (m, ϵ, l_0), it is implied in the definition of l and v_{th} as described in the scaling argument. The scaling of the kernel K with most of the system parameters $\{m, \epsilon, l_0, T, \rho\}$ means that effectively

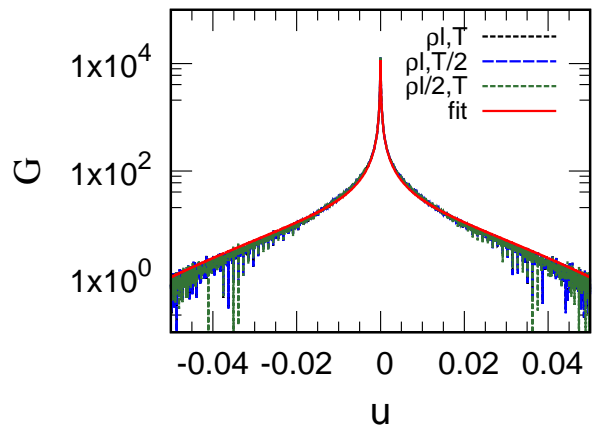


FIG. 4. $G_{0 \rightarrow u}$ for different values of T and ρl . The height and shape of all curves are identical which demonstrates the universal scaling. A fitting function $\frac{\alpha}{|u|^\beta} e^{-u^2/2\sigma^2}$ is also plotted and explained in Sec. IV E.

we only need to simulate one representative case for different values of the remaining parameters $\{u', n\}$ in order to cover the whole parameter space. We implement this idea in a later section.

Using the generated values for G in Fig. 4, the rate Γ in Eq. (19) can be computed using Eq. (11) and Eq. (23) as the rate of change of the variance of h :

$$\begin{aligned} \Gamma &= \left. \frac{d\langle (u - u')^2 \rangle_h}{dt} \right|_{t=0} \\ &= \rho^2 l v_{th} \sum_{j=-\infty}^{j=\infty} G_{u' \rightarrow u_j} (u_j - u')^2 \Delta u \\ &= a_n \rho^2 l v_{th}, \end{aligned} \quad (24)$$

so the proportionality constant a_n is given by the variance of G :

$$a_n = \langle (u - u')^2 \rangle_G. \quad (25)$$

C. MD and Boltzmann Evolution Comparison

To show that the kernel, K , contains the information of the thermalization dynamics, we use it to evolve $h(v, 0) = \delta(v)$ according Eq. (11) and compare the evolved distribution to that of the MD simulation. We tested several values of the evolution time t_f and different values for the system parameters. When N is big and ρ is small, the Boltzmann and the MD evolved distributions are in agreement as shown in Fig. 5. This demonstrates that the collision kernel, K , describes the thermalization process in the low density limit. For the comparison presented here, we use system parameters $N = 161$, $R = 51200 \mu\text{m}$, $l_0 = 1 \mu\text{m}$, $n = 6$, $\epsilon = 1 \text{ eV}$, $kT = 100 \text{ meV}$, $m = m_e$, and $t_f = 12800 \text{ ns}$

$1.6 \times 10^{-4}/\Gamma$, where Γ is computed from Eq. (19) using $\rho = (N - 1)/(2\pi R) \approx 0.5 \text{ mm}^{-1}$.

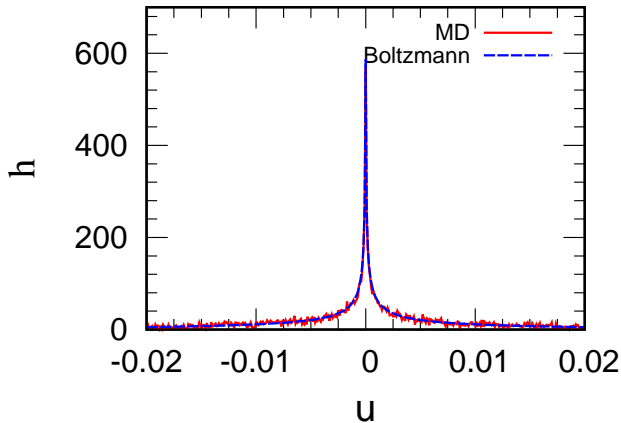


FIG. 5. MD and Boltzmann evolved distributions are in agreement. See text for relevant simulation parameters.

For smaller N or bigger ρ , we get a slight disagreement between the two methods. Four-body collisions are significant when ρ becomes large, which is not accounted for in the collision kernel, K . Moreover, at fixed ρ , the MD simulations require large N for convergence because the perturbation, h , has a large effect on the thermal particles for smaller N .

Equipped with the kernel, we can evolve the system for longer times using the Boltzmann Eq. (11). First, we calculated the kernel for a slow moving special particle $u' = -0.25$ and found the kernel G is approximately translation invariant as later demonstrated in Fig. 8. That is,

$$G_{0 \rightarrow u} \approx G_{u' \rightarrow u'+u}. \quad (26)$$

for $|u'| \ll 1$. Therefore, the only information needed to propagate small velocities to good accuracy is $G_{0 \rightarrow u}$. In this limit, the change in h during successive time steps in Eq. (10) becomes a repeated convolution integral.

Figure 6 shows the evolution of the delta perturbation over a time scale $t_f = 0.01/\Gamma$ as computed from the Boltzmann Eq. (10). The system's parameters are $N = 161$, $R = 51200 \mu\text{m}$, $n = 6$, $\epsilon = 1 \text{ eV}$, $kT = 100 \text{ meV}$, $m = m_e$, where Γ is computed from Eq. (19) and $\rho = (N - 1)/(2\pi R)$. At early times $t_f \Gamma < 1 \times 10^{-3}$, h has a cusp maximum which resembles that of G . That is because the change in h is approximately proportional to G as in Eq. (9) when G is highly localized. At later times $t_f \Gamma \sim 1 \times 10^{-2}$, the cusp flattens out as repeated convolutions relax the population to a Gaussian distribution, which subsequently spreads at a steady rate during the range of time considered. The relaxation to a Gaussian is a consequence of the repeated convolution and the Central-Limit theorem[18].

The spread of the perturbation in Fig. 6 indicates that its variance (which is proportional to the energy) is

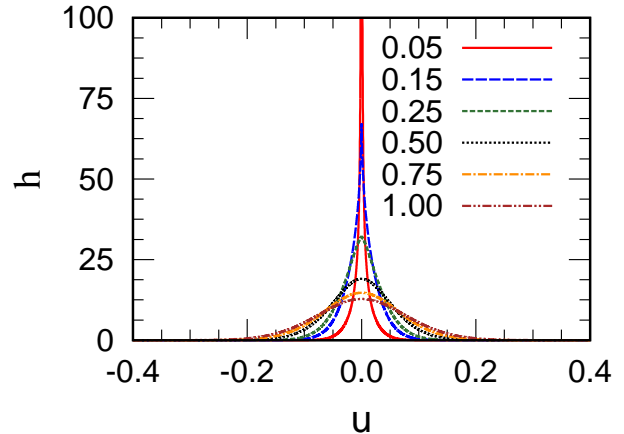


FIG. 6. Evolution of the perturbation, $h(u, t)$, at different times and approach toward equilibrium. Gas parameters are $N = 161$, $n = 6$, $R = 51200 \mu\text{m}$, $\epsilon = 1 \text{ eV}$ and $kT = 100 \text{ meV}$, m is the mass of the electron. Figure legends represent the time for the distribution in fraction of $0.01/\Gamma$, where Γ is computed from Eq. (19). There are two stages for the peak of the perturbation: non-Gaussian cusp and smooth Gaussian.

growing with time which is shown in Fig. 7. The linear evolution of the perturbation's energy in the time range considered suggests modelling the thermalization process as a random walk of the velocity u' of the special particle. The standard deviation of h is proportional to \sqrt{t} , just like the standard deviation of displacement in a random walk is proportional to the square root of the number of steps taken.

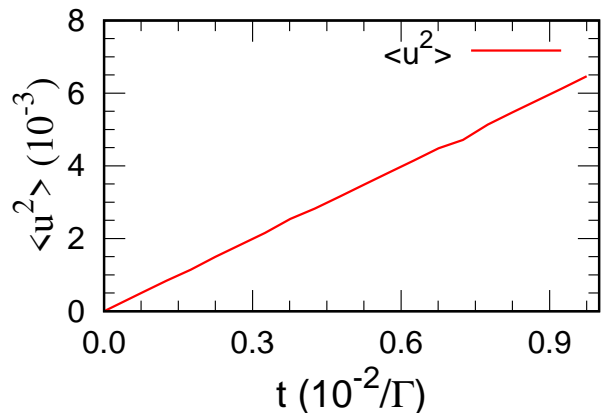


FIG. 7. The variance $\langle u^2 \rangle_h$ of the perturbation growing linearly with time. The evolution of h itself is plotted in Fig. 6.

Each 3-body collision with the thermal particles gives the special velocity a random kick leading to a random walk in velocity space. Using the order of magnitude of a_n in Tab. I, it takes $\sim 1/a_n \sim 10^4$ kicks to thermalize, i.e., the variance $\langle u^2 \rangle$ approaching 1. The kick magnitude is $\sim \sqrt{a_n} \sim 0.01$, which is of the order of magnitude of

the strongest kick in a 3-body collision (as explained in Sec. IV E).

D. G for a moving special particle $u' \neq 0$

In this section, we demonstrate how other velocity perturbations $u' \neq 0$ (moving special particles) scatter within the bath due to 3-body collisions. Since the kernel is proportional to the transition rates, Fig. 8 shows that a perturbation near the tail of the Maxwell-Boltzmann distribution at $u' = -3.0$ scatters to neighboring velocities more rapidly than from $u' = 0$. On the other hand, scattering from small velocities such as $u' = -0.25$ is almost identical to $u' = 0$.

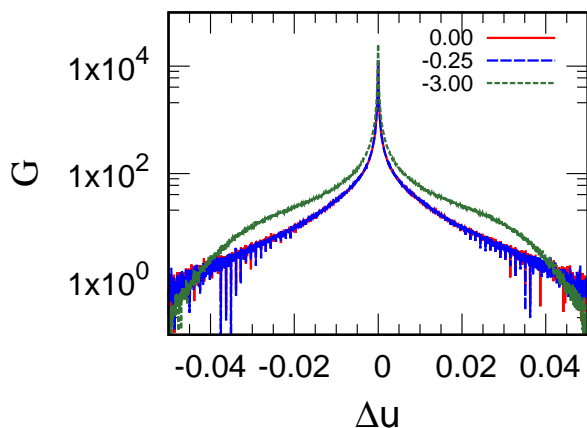


FIG. 8. Kernel G for different special velocities. A perturbation at the tail scatters faster than a perturbation at the center. The $u' = -3.0$ curve is slightly skewed to the right as shown in the first moment $\langle u \rangle$ in Fig. 9. The x -axis here is $\Delta u = u - u'$.

For several values of u' , the initial rate of change of the mean scaled velocity $d\langle u \rangle/dt$ and the variance $d\langle (u - u')^2 \rangle/dt$ are calculated as in Eq. (24) and are shown in Fig. 9. In particular, negative velocity perturbations have a positive initial rate of change of the average, which is a drag effect that slows down the special velocity. Also, we note that the initial rate of change of the variance only changes by a factor of ~ 2 . This indicates that the definition of Γ in Eq. (8) leads to a reasonable estimate of the time required for thermalization (i.e., Γ does not strongly depend on u').

From the $\langle (\Delta u)^2 \rangle$ curve, bigger velocity perturbations transition faster to neighboring velocities. This is an indication of detailed balance [19] which we numerically checked for pairs of velocity states. For example, the bins at $u = -3.00$ and $u = -2.96$ exchange populations at rates compatible with the steady state Maxwell-Boltzmann distribution. That is, for $n = 6$ we numerically found that

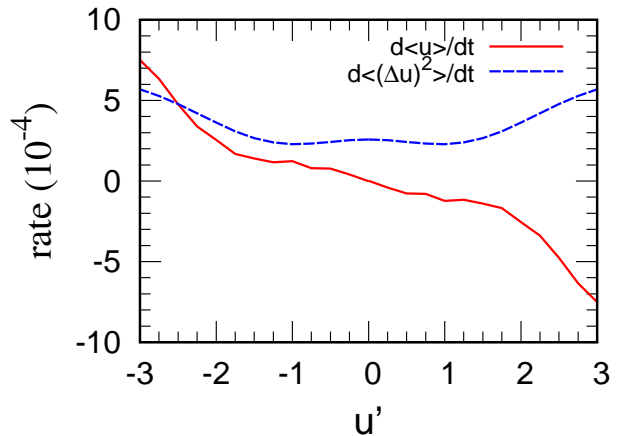


FIG. 9. Initial rate of change (scaled by $\rho^2 l v_{th}$) of the first moment $\langle u \rangle$ and the variance $\langle (u - u')^2 \rangle$ for perturbations localized at different velocities. The calculations were done for negative u' , but were reflected to extend over positive u' for clarity. The small fluctuations in the curves are due to statistical noise.

$$\frac{G_{-3.00 \rightarrow -2.96}}{G_{-2.96 \rightarrow -3.00}} = 1.12 \pm 0.04, \quad (27)$$

while the ratio between the Maxwell-Boltzmann population at the corresponding bins is $e^{-2.96^2/2}/e^{-3.00^2/2} = 1.13$.

E. Dependence of G on the Potential Power n

Figure 10 shows how the kernel compares for different powers n in the inverse power potential, Eq. (1). The scaled kernel is generally smaller for bigger n , indicating that the special particle scatters more slowly when the potential is steeper. Particularly, in the limit $n \rightarrow \infty$, the potential in Eq. (1) approaches hard walls at $|d| = l_0$, and the binary collision is an instantaneous velocity swap of two particles of size $2l_0$. In such limit, a ternary coincidence (Eq. (22)) necessary for thermalization is impossible. This is reflected in the decrease of a_n with increasing n , where the values of a_n computed using Eq. (25) are shown in Tab. I.

To understand why the kernel has its shape and why different values of n produce different shapes, we fitted the kernel guided by the details of the MC simulation. In Fig. 8, the kernel $G_{-3.0 \rightarrow -3.0 + \Delta u}$ near $\Delta u = 0$ decreases rapidly with increasing $|\Delta u|$, and decreases more rapidly for $|\Delta u| > \sim 0.03$. To capture both of these features, G can be fitted to a Gaussian modulated power law:

$$g(u) = \frac{\alpha}{|u|^\beta} e^{-u^2/2\sigma^2} \quad (28)$$

as shown in Fig. 4 for $n = 6$. The parameters α , β , and σ are shown for several values of n in Tab. I. The α

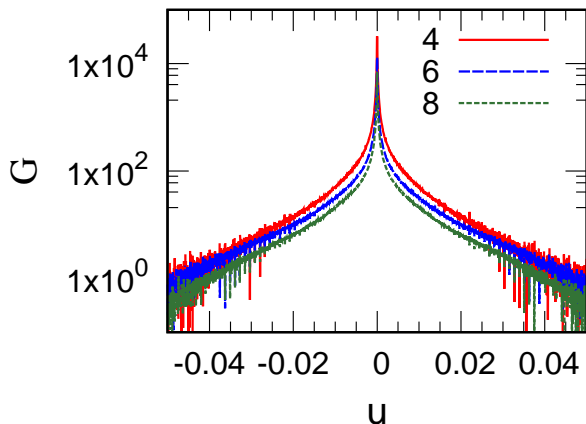


FIG. 10. The collision kernel $G_{0 \rightarrow u}$ for different potential power n values. $G_{0 \rightarrow u}$ is generally bigger for smaller n for the range of u shown.

parameter is proportional to the over all scattering rate $K_{0 \rightarrow 0}$, Eq. (12), and the power β measures how fast the kernel drops with increasing $|u|$ near $u = 0$ as in Fig. 4. We observe that both α and β decrease as n increases (i.e., when the potential is becoming steeper and approaching hard walls).

The choice of such fitting function can be explained by inspecting mono-energetic collisions in which the incoming energies are fixed as opposed to having a continuous ‘thermal’ distribution. Figure 11 shows the effect on the special particle starting from zero velocity in two launching cases: a symmetric case $v_2 = v_{th}$, $v_3 = -v_{th}$, and an asymmetric case $v_2 = 1.1v_{th}$, $v_3 = -0.9v_{th}$. The final kick the special particle receives, u_{1f} , is plotted against the delay Δt between launching particles 2 and 3. Both curves look similar with long tails for $|\Delta t| \gtrsim 3l/v_{th}$. The long tails happen because a large delay results in a tiny momentum transfer to the special particle. They are responsible for the fast drop of the kernel $G_{0 \rightarrow u}$ around $u = 0$, which is captured in the power-law term of the fitting function g . Moreover, both curves peak at a maximum momentum transfer $u_{1f,max} \sim 0.03$. The Gaussian modulation term in Eq. (28) is a way to average over the distribution of the launched particles from the thermal environment. Its width σ is not of order 1 but rather reflects the value of the fractional momentum transfer $u_{1f,max}$. In particular, σ correlates with $|u_{1f,max}|$; they both peak at $n = 6$ and drop monotonically away from $n = 6$ as shown in Tab. I.

For $n = 2$, $|u_{1f,max}|$ was found to be $\approx 1 \times 10^{-7}$ which is not different from 0 within errors resulting from the numerical solution of the equations of motion, Eq. (20). In fact, for the inverse square power potential it was shown that the equations of motion are integrable and the potential is, surprisingly, isospectral (momenta only trivially swap) [14]. That means that a system with such pairwise interaction can only thermalize through four or higher body collisions.

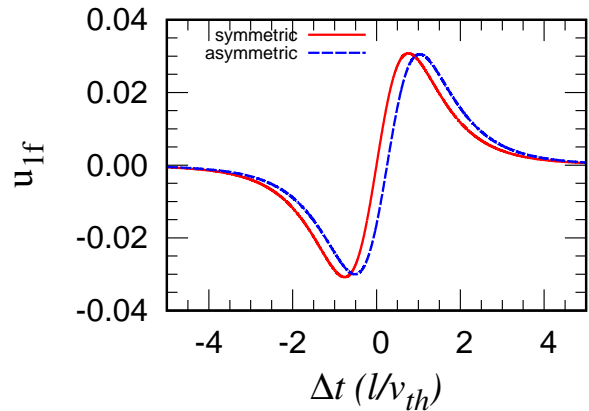


FIG. 11. Scaled kick u_{1f} as a function of the scaled delay Δt (in units of l/v_{th}) between launches. The symmetric case is for $u_{2i} = 1$ and $u_{3i} = -1$, while the asymmetric case is for $u_{2i} = 1.1$ and $u_{3i} = -0.9$. The curve for the asymmetric case was shifted horizontally for clarity. Both curves have long tails and peak at $u_{1f,max} \sim 0.03$.

TABLE I. Rate constants a_n and fitting parameters for different potential powers n . The uncertainty in α , β , and σ is ± 0.001 .

n	a_n	α	β	σ	$ u_{1f,max} $
2	0	0.000			1×10^{-7}
4	3.49×10^{-4}	0.237	1.182	0.022	2.69×10^{-2}
6	2.58×10^{-4}	0.182	1.117	0.027	3.06×10^{-2}
8	1.62×10^{-4}	0.148	1.076	0.025	2.76×10^{-2}
10	1.02×10^{-4}	0.129	1.046	0.021	2.37×10^{-2}
12	6.55×10^{-5}	0.115	1.023	0.018	2.04×10^{-2}

F. Broken Scaling in Lennard-Jones potential

In contrast with the inverse power law potential in Eq. (1), the Lennard-Jones potential is

$$U_{LJ}(d) = \epsilon \left[\left(\frac{l_0}{d} \right)^{12} - \left(\frac{l_0}{d} \right)^6 \right]. \quad (29)$$

This potential is different from the inverse power potential in important ways. First, it is attractive at long distance. Moreover, there is possibility of 3-body recombination. Most importantly, the scaling of the inverse power potential is lost in the Lennard-Jones potential. That is, we cannot fix the potential energy scale to kT as we did in Eq. (14).

Figure 12 shows $G_{0 \rightarrow u}$ for the Lennard-Jones potential for three different temperatures $kT = 0.1, 0.8$, and $10 eV$. In all cases, the potential energy scale $\epsilon = 1 eV$. When the kinetic energy (kT) is small compared to the potential energy, the scaled $G_{0 \rightarrow u}$ is almost the same for different temperatures as seen in the 0.1 and 0.8 eV curves. When the kinetic energy is larger, $G_{0 \rightarrow u}$ has a

significantly different shape as seen in the 10 eV curve. This shows the universal scaling (compare to Fig. 4) remains approximate at low T but is lost at high T . The simulation parameters are the same as those used for Fig. 4. The G kernel here is still scaled by l defined through Eq. (15) with $n = 6$. For $kT = 100$ meV, the dimensionless thermalization rate a_n is found to be 3.00×10^{-4} , which is bigger than that of the power law potential with $n = 6$ by 16%. Thus, the Lennard-Jones potential gives qualitatively similar thermalization rates to the inverse power potential even with the differences noted above.

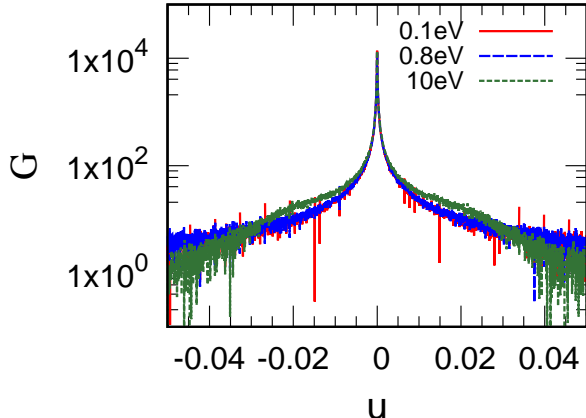


FIG. 12. Scaled collision kernel for different kT with $\epsilon = 1$ eV and other parameters from Sec. IV B. The small temperature curves overlap, but the high temperature curve deviates indicating the lack of scaling symmetry.

It is interesting to compare the rate of 3-body recombination to the rate of thermalization for 1D and 3D gases. In the present 1D gas, both processes involve three particles, and their rates scale like ρ^2 . In dilute 3D gases, thermalization is a 2-body process (with rate $\propto \rho$) and happens at a much faster rate than 3-body recombination. Moreover, for fixed ρ in our 1D gas, we find that the ratio of 3-body recombination rate to thermalization rate drops rapidly with increasing T . This could be explained by noting that at low T , a pair of particles approaching each other from far distance have small positive relative energy. If a third particle interact with the pair, there is a high chance that the energy of the pair transfers to the third particle, leaving the pair in a bound state with negative relative energy. At high T , the chances of the third particle taking away enough energy to switch the sign of the energy of the pair is small.

V. CONCLUSION

We have studied the rates of classical three-body thermalization in dilute one-dimensional gases with inverse power law interaction with $n > 2$ for various system parameters. Through MD simulations of the N -body gas and MC simulations of the 3-body scattering kernel, we

showed that the gas relaxes with a rate proportional to $\rho^2 \sqrt{\frac{kT}{m}} l_0 (\frac{\epsilon}{kT})^{\frac{1}{n}}$. The scaling of the thermalization rate in terms of T is exact for the inverse power potential, but only approximate at low T for the Lennard-Jones potential.

Classical 3-body thermalization in 1D is significantly slow (compared to higher dimensional gases) not only due to the ρ^2 scaling, but also the smallness of the proportionality constant, which comes from the weak redistribution of energy in each collision. The implication is that dilute 1D gases preserve their out-of-equilibrium states for a relatively long time. For example, a 1D Nitrogen atom gas with $\rho = 1$ atom/ $10 \mu m$ at $T = 10$ K interacting under the Nitrogen-Nitrogen Lennard-Jones potential takes around 10s to thermalize according to Eq. (24) and parameters found in [20].

By rewriting the equations of motion in a dimensionless way, we provided arguments for the scaling of both MD and MC simulations, which we verified numerically. Moreover, we have shown that the Boltzmann equation using a three-body collision kernel is sufficient to reproduce the evolution of low density N -body gas calculable from MD simulations. Additionally, the collision kernel behaves like a power law for small momentum transfer. For bigger momentum transfer, it is modulated by a Gaussian with width of order of the maximum momentum transfer during a mono-energetic collision. Finally, the collision kernel provided us with an understanding of how the overall rates and the statistical details of three-body scattering depend on the potential power n .

ACKNOWLEDGMENTS

This work was supported by the US Department of Energy, Office of Science, Basic Energy Sciences, under Award No. DE-SC0012193.

Appendix A: Molecular Dynamics Simulation

In this appendix, we provide details and analysis of the MD simulations. To simulate the gas of N particles in Fig. 1, the initial velocities are chosen as per Eq. (5), whereas the initial locations are chosen randomly according to a relative potential energy Boltzmann factor. We evolve the system from time $t_i = 0$ to time t_f according to Eq. (13) using Runge-Kutta methods with adaptive time step [21]. At t_f , we subtract the background thermal distribution as per Eq. (5) to single out the perturbation $h(v, t_f)$. We average over many trajectories and a window of time around t_f to reduce the statistical noise.

The number of terms in the force calculation in Eq. (13) scales like N^2 for a single time step, which makes it difficult to simulate more than 30 particles. To decrease the computational time, we utilize that the inverse power potential in Eq. (1) is relatively ‘short-range’ for

$n \geq 2$ and small density ρ . In this regime, particles are only interacting significantly with their close neighbors, while the interaction with further particles can be ignored. This allows us to do nearest neighbors calculations for the force, which results in a time complexity that scales like N . The neighbors are selected by ordering the particles according to their initial locations. For 3 nearest neighbors, for example, particle number 5 experiences a force from particles numbered 2-4 and 6-8. Since the potential is infinitely repulsive at short distance, the particles cannot pass through each other and the particle order is fixed. We checked that the results converged for 3 nearest neighbors which was used for all MD simulations in this paper. Using this method, we could simulate more than 160 particles.

To ensure that 3-body collisions are the largest effect, we choose a small density $\rho = (N - 1)/2\pi R$. We verify the ρ^2 scaling by simulating a density ρ for time t_f and comparing the final h to that of another simulation with $\rho/2$ (by doubling R for a given N) for time $4t_f$. The results converge for densities near ($\rho l \sim 1 \times 10^{-3}$). From analysis of the Runge-Kutta with adaptive time step algorithm, the related best-case time complexity scales like $1/\rho$.

Once we fix the convergence density, we double N and R in steps to obtain thermodynamic convergence. The results converge for particle number near $N = 160$. Once we fix the convergence particle number, we run the simulation for a longer time to get appreciable evolution of h . All these considerations combined render the MD simulations computationally expensive, and we chose to limit the simulation time to t_f of the order $1 \times 10^{-4}/\Gamma$, where Γ is from Eq. (19).

Appendix B: Boltzmann Equation

In the kinetic theory of gases, the state of a gas in 1D is described by the aggregate one-particle distribution in coordinate-velocity space $f(x, v, t) dx dv$. The evolution of such distribution is described by the Boltzmann equation [22]:

$$\frac{\partial f}{\partial t} + v \frac{\partial f}{\partial x} + \frac{f}{m} \frac{\partial f}{\partial v} = \left(\frac{\partial f}{\partial t} \right)_c, \quad (\text{B1})$$

where f is the external force and m is the mass of the particle. For an isolated system with uniform density ρ , which we assume in our work, the velocity and space derivative terms drop out. In this case, the only way to change f is through inter-particle interactions dictated by the collision term on the right hand side. (Henceforward, we use f to represent the distribution in velocity only. The one-particle velocity-space distribution is ρf , where ρ is the number density.) The collision term is modelled and computed in the MC simulation in Appendix C.

Appendix C: Monte Carlo Simulation

In this Appendix, we provide the relevant distributions and steps of the Monte Carlo Algorithm for generating the discrete version of $K_{v' \rightarrow v}$. First, we treat the case of an initially stationary special particle, $v' = 0$. The one-particle phase space thermal distribution is given by ρf_0 where f_0 is the equilibrium velocity distribution in Eq. (4). At $x = L/2$, particles are entering the observation region with negative velocity. The rate of entry is equal to the probability current (flux) $\rho f_0 |v|$ integrated from $v = -\infty$ to 0. We get the same rate from the left. So overall we get a rate of

$$r = \int_{-\infty}^{+\infty} \rho f_0(v) |v| dv = \rho v_{th} \sqrt{\frac{2}{\pi}}, \quad (\text{C1})$$

and a velocity distribution of the launched particles

$$P_{launch}(v) = \rho f_0(v) |v| / r, \quad (\text{C2})$$

which is the probability that v lies between $v - dv/2$ and $v + dv/2$ per dv (normalized so the integral over all v is 1).

To treat the case $v' \neq 0$, we go to the reference frame moving with v' . The distribution in that frame is $\rho f_0(v + v')$; therefore, the launching rate is generally

$$\begin{aligned} r &= \int_{-\infty}^{\infty} \rho f_0(v + v') |v| dv \\ &= \frac{\rho v_{th}}{\sqrt{2\pi}} \int_{-\infty}^{\infty} e^{-(u+u')^2} |u| du \\ &= \frac{\rho v_{th}}{\sqrt{2\pi}} \left[2e^{-\frac{u'^2}{2}} + \sqrt{2\pi} u' \operatorname{erf} \left(\frac{u'}{\sqrt{2}} \right) \right], \quad (\text{C3}) \end{aligned}$$

where erf is an error function. The general launch distribution for velocity is

$$P_{launch}(v) = \rho f_0(v + v') |v| / r. \quad (\text{C4})$$

The rate r determines the probability distribution for a delay time between the launching of particles 2 and 3:

$$P_{delay}(\Delta t) = r e^{-r \Delta t}. \quad (\text{C5})$$

Using these distributions, we implement the MC simulation as follows: 1) At time $t = 0$, particle 1 is initialized at $x = 0$ with $v_1 = 0$. 2) Particle 2 is initialized with a random velocity v_2 picked from the distribution $P_{launch}(v)$ in Eq. (C4) at $x = \pm L/2$ depending on the sign of v_2 . 3) Particle 3 is initialized with a random velocity v_3 picked from the distribution $P_{launch}(v)$ at $x = \pm L/2$ depending on the sign of v_3 , with a random time delay Δt chosen according to $P_{delay}(\Delta t)$ in Eq. (C5). 4) The 3 initial velocities v_1 , v_2 , and v_3 are added to the appropriate bins (histogram) of the discretized approximation of K , Eq. (11), with a value of -1 because these velocities are destroyed through the collision.

5) Using Runge-Kutta methods, the particles are propagated until they collide and separate appreciably. 6) The final velocities w_1 , w_2 , and w_3 are added to the histogram with a +1 because these velocities are created. 7) Steps 1-6 are repeated for a number of trajectories N_{traj} until the statistical noise decreases to a sufficient level. 8) The histogram is divided by $N_{traj}t_{avg}\Delta v$ where t_{avg} is the inverse of the rate r . This discretized approximation converges to $K_{v'\rightarrow v'+v}$ in the limit $N_{traj} \rightarrow \infty$ and $\Delta v \rightarrow 0$.

This prescription is a Monte Carlo evaluation of the scattering kernel where our delta-perturbative model of the collision term can be read from Eq. (10) as

$$\left(\frac{\partial h}{\partial t}\right)_c = \int_{-\infty}^{\infty} K_{v'\rightarrow v} h(v', t) dv', \quad (C6)$$

where K is computed from the MC simulation. For $v' = 0$,

$$\begin{aligned} K_{0\rightarrow v} = & \int \int \int dv_2 dv_3 d\Delta t \frac{\rho f_0(v_2)|v_2|}{r} \frac{\rho f_0(v_3)|v_3|}{r} \\ & \times r e^{-r\Delta t} \times r [-\delta(v) - \delta(v_2 - v) - \delta(v_3 - v) \\ & + \delta(w_1 - v) + \delta(w_2 - v) + \delta(w_3 - v)]. \end{aligned} \quad (C7)$$

where w_1, w_2, w_3 are the outgoing velocities of the collision and are functions of the incoming velocities v_2, v_3 and the time delay Δt . r is the rate of launching in Eq. (C1), and f_0 is the Maxwell distribution in Eq. (4). The first three terms in the integrand are the normalized distributions (integral over the respective domain being 1) of v_2, v_3 , and Δt . The last term ($r \times$ the square bracket) is the rate of destruction subtracted from the rate of creation of velocity v . For special velocity $v' \neq 0$, we get a similar integral expression but with the velocity arguments shifted as in Eq. (C4) and r defined in Eq. (C3).

Our collision term is comparable to that in Ref. [10] which is derived for 2-body collisions in 3D using the differential cross-section. It is also comparable to that in Ref. [15], which handles 3-body collisions in 1D but assumes constant transition rates for all $v_1, v_2, v_3 \rightarrow w_1, w_2, w_3$ interactions compatible with energy and momentum conservation. The collision term in Ref. [15] yields an analytically solvable Boltzmann Equation, but is not derivable from an inter-particle interaction.

-
- [1] J. Christen, M. Grundmann, E. Kapon, E. Colas, D. Hwang, and D. Bimberg, Ultrafast carrier capture and long recombination lifetimes in GaAs quantum wires grown on nonplanar substrates, *Appl. Phys. Lett.* **61**, 67 (1992).
- [2] K. H. Baloch, N. Voskanyan, M. Bronsgeest, and J. Cummings, Remote Joule heating by a carbon nanotube, *Nat. Nanotechnol.* **7**, 316 (2012).
- [3] T. O'Neil and P. Hjorth, Collisional dynamics of a strongly magnetized pure electron plasma, *Phys. Fluids* **28**, 3241 (1985).
- [4] S. Erne, R. Bückner, T. Gasenzer, J. Berges, and J. Schmiedmayer, Universal dynamics in an isolated one-dimensional Bose gas far from equilibrium, *Nature* **563**, 225 (2018).
- [5] M. Moško and V. Cambel, Thermalization of a one-dimensional electron gas by many-body Coulomb scattering: Molecular-dynamics model for quantum wires, *Phys. Rev. B* **50**, 8864 (1994).
- [6] F. Haldane, 'Luttinger liquid theory' of one-dimensional quantum fluids. i. properties of the Luttinger model and their extension to the general 1d interacting spinless Fermi gas, *J. Phys. C Solid State* **14**, 2585 (1981).
- [7] R. Livi, Anomalous transport in low-dimensional systems: A pedagogical overview, *Physica A*, 127779 (2022).
- [8] L. Rota, F. Rossi, S. Goodnick, P. Lugli, E. Molinari, and W. Porod, Reduced carrier cooling and thermalization in semiconductor quantum wires, *Phys. Rev. B* **47**, 1632 (1993).
- [9] M. Panfil, S. Gopalakrishnan, and R. M. Konik, Thermalization of interacting quasi-one-dimensional systems, *Phys. Rev. Lett.* **130**, 030401 (2023).
- [10] G. Uhlenbeck, G. Ford, and E. Montroll, *Lectures in Statistical Mechanics: By G.E. Uhlenbeck and G.W. Ford; with an Appendix on Quantum Statistics of Interacting Particles by E.W. Montroll*, Lectures in applied mathematics (American Mathematical Society, 1963).
- [11] L. D. Landau and Lifshitz, *Statistical Physics* (Butterworth-Heinemann, 1981).
- [12] J.-B. Fouvry, P.-H. Chavanis, and C. Pichon, Kinetic theory of one-dimensional homogeneous long-range interacting systems with an arbitrary potential of interaction, *Phys. Rev. E* **102**, 052110 (2020).
- [13] A. J. Maciejewski and M. Przybylska, Non-integrability of the three-body problem, *Celest. Mech. Dyn. Astr.* **110**, 17 (2011).
- [14] F. Calogero and C. Marchioro, Exact solution of a one-dimensional three-body scattering problem with two-body and/or three-body inverse-square potentials, *J. Math. Phys.* **15**, 1425 (1974).
- [15] S. K. Ma, One-dimensional Boltzmann equation with a three-body collision term, *J. Stat. Phys.* **31**, 107 (1983).
- [16] J.-B. Fouvry, B. Bar-Or, and P.-H. Chavanis, Kinetic theory of one-dimensional homogeneous long-range interacting systems sourced by $1/N^2$ effects, *Phys. Rev. E* **100**, 052142 (2019).
- [17] D. P. Kroese, T. Taimre, and Z. I. Botev, *Handbook of Monte Carlo methods* (John Wiley & Sons, 2013).
- [18] A. Klenke, *Probability theory: a comprehensive course* (Springer Science & Business Media, 2013).
- [19] A. Gorban, Detailed balance in micro-and macrokinetics and micro-distinguishability of macro-processes, *Results Phys.* **4**, 142 (2014).

- [20] B. Mamedov and E. Somuncu, Analytical treatment of second virial coefficient over Lennard-Jones (2n - n) potential and its application to molecular systems, *J. Mol. Struct.* **1068**, 164–169 (2014).
- [21] W. H. Press, *Numerical recipes 3rd edition: The art of scientific computing* (Cambridge university press, 2007).
- [22] R. Zwanzig, *Nonequilibrium Statistical Mechanics* (Oxford Univ. Press, 2009).